Journal of Magnetic Resonance 204 (2010) 290–302

Contents lists available at ScienceDirect

Journal of Magnetic Resonance

journal homepage: www.elsevier.com/locate/jmr

Quantitative determination of NOE rates in perdeuterated and protonated proteins: Practical and theoretical aspects

Beat Vögeli [a], Michael Friedmann [a], Dominik Leitz [a], Alexander Sobol [a], Roland Riek [a,b,*]

[a] Laboratory of Physical Chemistry, Swiss Federal Institute of Technology, ETH-Hönggerberg, CH-8093 Zürich, Switzerland
[b] The Salk Institute, 10010 N. Torrey Pines Road, La Jolla, CA 92037, USA

ARTICLE INFO

Article history:
Received 21 December 2009
Revised 10 March 2010
Available online 15 March 2010

Keywords:
Backbone motion
Nuclear Overhauser Effect
NOE
NOESY
Ubiquitin
GB3
Protein dynamics

ABSTRACT

Precision and accuracy are the limiting factors in extracting structural and dynamic information from experimental NOEs. In this study, error sources at all stages of such an analysis are identified and errors are estimated. The data set of H^N–H^N cross-relaxation rates obtained from triple-labeled ubiquitin presented in [B. Vögeli, T.F. Segawa, D. Leitz, A. Sobol, A. Choutko, D. Trzesniak, W. van Gunsteren, R. Riek, J. Am. Chem. Soc. 131 (47) (2009) 17215–17225] is extended to rates obtained from a double-labeled sample. Analog data sets are presented for GB3. It is shown that quantitative NOE rates can be determined with high accuracy from both triple-labeled as well as double-labeled samples. The quality of experimental cross-relaxation rates obtained from 3D HXQC–NOESY and NOESY–HXQC experiments is discussed. It is shown that NOESY–HXQC experiments provide rates of the same quality as HXQC–NOESY if both diagonal and cross peaks for a spin pair can be resolved. Expressions for cross-relaxation rates for anisotropically tumbling molecules exhibiting fast and slow motion are derived. The impact of anisotropy on the prediction of cross-relaxation rates and on the conversion of experimental rates into effective distances is discussed. For molecules with anisotropy $D_{\parallel}/D_{\perp}$ up to five the distance error is smaller than 2%. Finally, "averaged order parameters" are calculated for specific secondary-structural elements showing similar trends for ubiquitin and GB3.

1. Introduction

It has recently been demonstrated that the measurement of NOE buildups [1,2] between amide protons in perdeuterated human ubiquitin enables the determination of H^N–H^N distances up to 5 Å with high accuracy and precision [3]. These NOE-derived distances have an experimental error of ≈0.07 Å, which is smaller than the pairwise root-mean-square deviation of 0.24 Å obtained with corresponding distances extracted from either an NMR or an X-ray structure, and also smaller than the pairwise rmsd between distances from X-ray and NMR structures (0.15 Å). The extension of this approach to all protons in a protein poses difficulties. In particular, in a protonated sample spin diffusion is much stronger. Errors introduced by spin diffusion are examined by comparing rates obtained from double and triple-labeled samples. Furthermore, the proton mixing element in the 3D ^{15}N-resolved HMQC–[^{1}H,^{1}H]–NOESY experiment has been placed before acquisition enabling convenient extraction of the cross-relaxation rates. However, the water suppression is based on a WATERGATE sequence [4] which also excites in part $^1H^{\alpha}$ protons and corresponding NOEs cannot be determined accurately. Such NOEs are of emergent interest and it is discussed how NOEs can be determined if an HXQC element (that is, HSQC or HMQC) is placed after the NOESY mixing time just preceding acquisition. The impact of diffusion anisotropy has been neglected in the study of ubiquitin [3]. This is justified by the relatively small ratio of the longitudinal and transverse axis of the diffusion tensor ($D_{\parallel}/D_{\perp} = 1.17$). While the error for experimental distances is very small, the error of cross-relaxation rates (and therefore order parameters) is no more than 5%. It is, however, important to get an estimate of errors for proteins with larger anisotropy. The effect is studied on the example of GB3 with a ratio of 1.4. Expressions for cross-relaxation rates for anisotropically tumbling molecules exhibiting fast and slow motion are derived.

2. Theory

2.1. Cross-relaxation rates

The time dependence of the peak intensities in a NOESY spectrum is determined by the following differential equation for N spins [5]:

* Corresponding author at: Laboratory of Physical Chemistry, Swiss Federal Institute of Technology, ETH-Hönggerberg, CH-8093 Zürich, Switzerland. Fax: +41 411 633 10 73.
E-mail address: roland.riek@phys.chem.ethz.ch (R. Riek).

1090-7807/$ - see front matter © 2010 Elsevier Inc. All rights reserved.
doi:10.1016/j.jmr.2010.03.009

$$\frac{d}{dt}I(t) = -RI(t) \tag{1}$$

I is an $N \times N$ matrix with the spectral intensities of the diagonal peaks at mixing time t as the matrix diagonal and those of the cross peaks as off-diagonal elements. The $N \times N$ relaxation matrix R contains autorelaxation rates ρ_K of spin K and cross-relaxation rates σ_{KL} between spins K and L and is formally obtained from the integrated form of Eq. (1):

$$R = \frac{\ln(I(t)I(0)^{-1})}{-t} \tag{2}$$

If a third spin M is far apart from K and L, $\sigma_{KM} = \sigma_{ML} = 0$. If this is true for all other spins in the system an exact analytical solution for the remaining 2-spin system KL can be obtained [3].

$$\frac{\Delta I_{KK}(t)}{\Delta I_{KK}(0)} = \frac{1}{2}\left[\left(1 - \frac{\rho_K - \rho_L}{\lambda_+ - \lambda_-}\right)e^{-\lambda_- t} - \left(1 + \frac{\rho_K - \rho_L}{\lambda_+ - \lambda_-}\right)e^{-\lambda_+ t}\right] \tag{3.1}$$

$$\frac{\Delta I_{KL}(t)}{\Delta I_{KK}(0)} = -\frac{\sigma_{KL}}{(\lambda_+ - \lambda_-)}[e^{-\lambda_- t} - e^{-\lambda_+ t}] \tag{3.2}$$

with

$$\lambda_\pm = \frac{(\rho_K + \rho_L)}{2} \pm \sqrt{\left(\frac{\rho_K - \rho_L}{2}\right)^2 + \sigma_{KL}^2} \tag{3.3}$$

These equations are convenient because every two-spin system can be independently evaluated in a simple fit. In practice, however, $\sigma_{KM}, \sigma_{ML} \neq 0$ and the assumption of an isolated two-spin system breaks down. The introduced error can be evaluated by a Taylor series of Eq. (1) to second order in t:

$$\frac{\Delta I_{KK}(t)}{\Delta I_{KK}(0)} = 1 - \rho_K t + \frac{1}{2}(\rho_K^2 + \sigma_{KL}^2 + \sigma_{KM}^2)t^2 \tag{4.1}$$

$$\frac{\Delta I_{KL}(t)}{\Delta I_{KK}(0)} = -\sigma_{KL} t + \frac{1}{2}[(\rho_K + \rho_L)\sigma_{KL} + \sigma_{KM}\sigma_{LM}]t^2 \tag{4.2}$$

In both equations the last terms containing σ_{KM} or σ_{ML} are the modifications due to an additional loss of K magnetization to spin M, and due to spin diffusion from K to L via M.

2.2. The impact of cross-correlated relaxation

Although the Solomon Eq. (1) is restricted to the N dimensional space of all single spin magnetization modes it is usually sufficient for the analysis of NOESY phenomena. More completely, multi-spin modes up to N spins may be included [35]. These modes are created from single spin modes via cross-correlated relaxation. Similarly to spin diffusion, they are involved in indirect pathways from spin I to spin S. The two most efficient pathways are via $2I_zS_z$ (first under interference of dipole (IS)/chemical shift anisotropy (CSA) of spin (I), then dipole(IS)/CSA(S)) and via $4I_zS_zK_z$ (first dipole(IS)/dipole(IK), then dipole(IS)/dipole(SK), respectively. As opposed to spin diffusion, for which all cross-relaxation rates scale with the spectral density function at zero frequency, all longitudinal cross-correlation rates are sampled at the proton larmor frequency, which results in very small contributions to the NOE under protein-typical rotational correlation times of several nanoseconds.

To quantify these small contributions, upper limits were calculated for GB3 with a NOESY mixing time of 60 ms. All the interaction main axes were assumed to be parallel or antiparallel in order to generate the maximally possible interaction strengths. Numerical integration of the complete equation for the three spin system ISK was used to estimate the (neglected) contribution of the cross-correlated relaxations in the NOE cross peaks between I and S for every spin K no further than 8 Å apart from both. The cumulative contributions are smaller than 1% for all the NOEs obtained from the double-labeled sample and even smaller for the triple-labeled sample. Generally, the largest relative contributions are obtained for the weakest NOEs. Furthermore, true cumulative contributions are expected to be much smaller because every contribution scales between −0.5 and 1 depending on the true angle between the interaction axes. Hence, contributions coming from cross-correlated relaxation can be neglected in the presented study on GB3. For ubiquitin, the errors due to the abandonment of cross-correlated relaxation are even smaller than those for GB3 since the molecular tumbling time is larger. Conclusively, the impact of cross-correlated relaxation can be neglected in this study.

2.3. The impact of partial deuteration and perdeuteration

Spin diffusion as described in Eqs. (4.1) and (4.2) is omnipresent and the NOE rates must be corrected for it. The extent of spin diffusion can be reduced drastically by perdeuteration. The deuteration level of a perdeuterated sample is typically ca. 99% for H^α and 95% for other carbon-bound protons. It has been shown that in most cases Eqs. (3.1)–(3.3) can be used to obtain H^N–H^N σ_{KL} [3]. For ubiquitin with a correlation time of 9.3 ns and NOESY mixing times of ≈100 ms, inclusion of all these additional pathways leads to an overestimation of NOE rates σ_{KL} of 10–50% in non-consecutive residues in the α helix and loops, and an averaged overestimation of only 9% in the other spin pairs. It has been suggested that this effect can be either corrected using a known 3D structure or by a uniform factor per secondary-structural element. However, it is very important to note that the perdeuteration level must be known. Fig. 1 shows the influence of residual aliphatic protonation on the determination of NOE rates between sequential amides in an α helix and a β sheet. It is obvious that accurate correction for spin diffusion fails in a sample that is deuterated (but not perdeuterated), which results in an overall deuteration level of ∼85% having a highly inhomogeneous distribution of deuterated/protonated sites [6,7]. The problem of an unknown percentage of residual protonation is absent in measurements with fully protonated proteins. In turn, spin diffusion is extensively active. To scope with it without the introduction of large structure-based correction factors the NOE mixing time has to be reduced drastically. Fig. 2 shows the

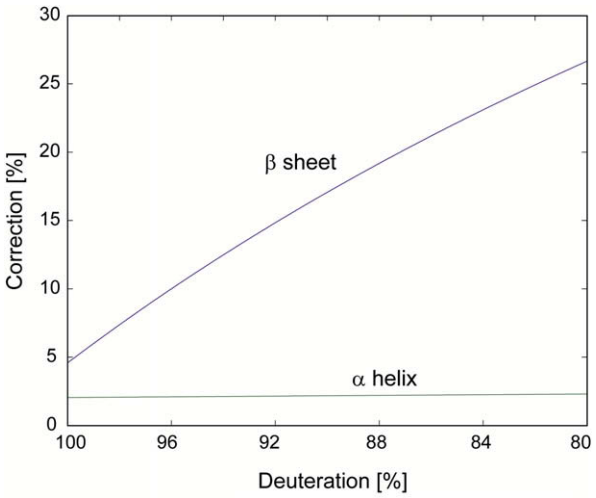

Fig. 1. Influence of residual aliphatic protonation on the determination of NOE rates between sequential amides in an α helix (gray line) and a β sheet (blue line). Corrections to apparent experimental cross-relaxation rates are calculated for spin pairs of amide protons of residues 15/16 and 27/28 of ubiquitin, assuming a mixing time t_{mix} = 100 ms and τ_c = 9.3 ns and fixing the deuteration level of all protons except for amide and H^α to 95%. (For interpretation of the references to color in this figure legend, the reader is referred to the web version of this article.)

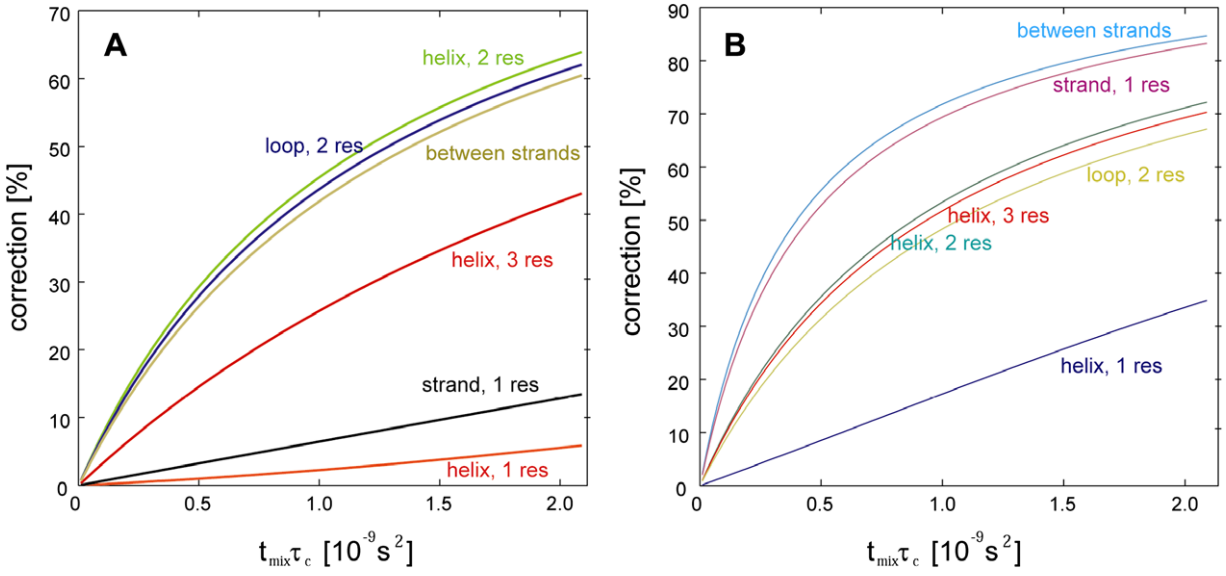

Fig. 2. Influence of spin diffusion on the determination of NOE rates between amide spin pairs in dependence of the NOE mixing time t_m and the rotational correlation time τ_c. Correction which must be applied to apparent experimental cross-relaxation rates are shown for a perdeuterated (A) and a protonated protein (B). Representative spin pairs from ubiquitin are selected. Spins in an α helix separated by 1, 2 and 3 residues are exemplified by spin pairs 27/28, 27/29 and 27/30, spins separated by 1 residue in a β strand by 15/16 and from different β strands by 2/15, and spins separated by 2 residues in a loop by 58/60. The ratio of τ_c and t_{mix} is fixed at 10^{-7}. For the perdeuterated protein, the deuteration level is assumed to be 99% for H^{α} and 95% for all other non-exchangeable protons. (For interpretation of the references to colour in this figure legend, the reader is referred to the web version of this article.)

correction factors needed in the determination of NOE rates between sequential and non-sequential amides in an α helix, a β sheet and a loop in dependence on the product of the mixing time t_{mix} and rotational correlation time τ_c (3D plots with τ_c and t_{mix} on the *x* and *y* axis, respectively, are provided in the Supporting Information). In the present study, a maximal mixing time of 60 ms was used for $^{13}C,^{15}N$-labeled GB3 ($\tau_c = 3.43$ ns) and 25 ms for $^{13}C,^{15}N$-labeled ubiquitin ($\tau_c = 9.3$ ns), respectively. Corrections of typically 30% to the apparent relaxation rates are required and Eqs. (3.1) and (3.2) are not valid anymore.

In addition, for an accurate determination of the NOE rates the extent of D_2O in the sample must be known. Because of the 95/5% and 97/3% H/D equilibria in the GB3 and ubiquitin samples the NOE rates must be corrected with uniform factors of 1/0.95 and 1/0.97, respectively. In principle, this residual deuteration may complicate the analysis of NOE rates further because it also influences the spin diffusion *via* amide protons and hence minimal addition of D_2O for locking is advantageous. On state-of-the-art spectrometers 3% D_2O is by far sufficient.

2.4. Cross-relaxation rates for isotropic tumbling

The homonuclear cross-relaxation rate is given by [8,9]

$$\sigma_{KL} = \left(\frac{\mu_0}{4\pi}\right)^2 \frac{\gamma^4 h^2}{40\pi^2} \frac{1}{\left(r_{KL}^{\text{rigid}}\right)^6} [J(0) - 6J(2\omega)] \tag{5}$$

where γ is the gyromagnetic ratio of nucleus *K*, ω is the spectral frequency of the nuclei, μ_0 is the permeability in vacuum, and *h* denotes Planck's constant. r_{KL}^{rigid} is the internuclear distance in a hypothetically rigid structure. A simple expression for the spectral density *J* is obtained under the assumption of isotropic molecular tumbling [10]

$$J(\omega) = S_{KL}^{\text{fast2}} \frac{\tau_c}{1 + (\tau_c\omega)^2} + \left(\left(r_{KL}^{\text{rigid}}\right)^6 \left\langle \frac{1}{r_{KL}^6} \right\rangle - S_{KL}^{\text{fast2}}\right) \frac{\tau_{\text{tot}}}{1 + (\tau_{\text{tot}}\omega)^2} \tag{6}$$

with

$$\frac{1}{\tau_{\text{tot}}} = \frac{1}{\tau_c} + \frac{1}{\tau_{\text{int}}} \tag{7}$$

where τ_c is the rotational correlation time of the molecule and τ_{int} is the correlation time for internal motion. The angled brackets denote a Boltzmann ensemble average. S_{XY}^{fast2} is an order parameter for fast internal motion [11],

$$S_{XY}^{\text{fast2}} \equiv \left(r_{XY}^{\text{rigid}}\right)^6 \frac{4\pi}{5} \sum_{q=-2}^{2} \left\langle \frac{Y_{2q}\left(\theta_{XY}^{\text{mol}}, \phi_{XY}^{\text{mol}}\right)}{(r_{XY})^3} \right\rangle^2 \tag{8}$$

An experimentally accessible order parameter which covers all time scales has been introduced [3]. It is defined by the true (experimental) cross-relaxation rate normalized to the one expected for a rigid molecule,

$$S_{KL}^2 \equiv \frac{\sigma_{KL}^{\text{exp}}}{\sigma_{KL}^{\text{rigid}}} \tag{9}$$

For macromolecules at high magnetic fields $J(\omega)$ sampled at frequencies other than zero can be neglected and S_{KL}^2 can be rewritten as

$$S_{KL}^2 = S_{KL}^{\text{fast2}} + \left(\left(r_{KL}^{\text{rigid}}\right)^6 \left\langle \frac{1}{r_{KL}^6} \right\rangle - S_{KL}^{\text{fast2}}\right) \frac{1}{1 + \tau_c/\tau_{\text{int}}} \tag{10}$$

For internal motion much faster than nanoseconds ($\tau_{\text{int}} \ll \tau_c$), S_{KL}^2 reduces to the order parameter of fast motion as defined in Eq. (8)

$$S_{KL}^2 = S_{KL}^{\text{fast2}} \tag{11.1}$$

For motion much slower than the molecular tumbling ($\tau_{\text{int}} \gg \tau_c$) S_{KL}^2 becomes independent of angular coordinates,

$$S_{KL}^2 = \left(r^{\text{rigid6}}\right) \left\langle \frac{1}{r^6} \right\rangle \tag{11.2}$$

The simplest and most common way to extract distances from the measured cross-relaxation rate is to use Eq. (5) under the assumption of a rigid molecule. Motional effects are absorbed into the distance which must be replaced by an effective distance r_{KL}^{eff}:

$$\sigma_{KL} = \left(\frac{\mu_0}{4\pi}\right)^2 \frac{\gamma^4 h^2}{40\pi^2} \frac{\tau_c}{\left(r_{KL}^{\text{eff}}\right)^6} \tag{12}$$

2.5. Cross-relaxation rates for anisotropic tumbling

If the molecule tumbles anisotropically, Eqs. (6)–(10), (11.1), (11.2), (12) have to be modified accordingly. The spectral density function is given by:

$$J(\omega) = \sum_{j=-2}^{2} C_j \left\{ S_{KL,j}^{\text{fast2}} \frac{\tau_j}{1+(\tau_c\omega)^2} + \left(\left(r_{KL}^{\text{rigid}}\right)^6 \left\langle \frac{1}{r_{KL}^6} \right\rangle - S_{KL,j}^{\text{fast2}} \right) \frac{\tau_{\text{tot},j}}{1+(\tau_{\text{tot},j}\omega)^2} \right\} \tag{13}$$

where $1/\tau_k$ are the eigenvalues of the anisotropic diffusion operator D [12,13]:

$$\begin{aligned} 1/\tau_2 &= 6(D + \sqrt{D^2 - D'^2}) \\ 1/\tau_{-2} &= D_x + D_y + 4D_z \\ 1/\tau_1 &= 4D_x + D_y + D_z \\ 1/\tau_{-1} &= D_x + 4D_y + D_z \\ 1/\tau_0 &= 6(D - \sqrt{D^2 - D'^2}) \end{aligned} \tag{14.1-5}$$

and the coefficients C_k contain the dependency on the vector K–L given by the polar angles θ and ϕ in the molecular frame:

$$C_2 = (r^{\text{rigid}})^6 \left\langle \frac{1}{r_A^3 r_B^3} \begin{pmatrix} \frac{3w^2}{4N^2} \sin^2\theta_A \sin^2\theta_B \cos 2\varphi_A \cos 2\varphi_B \\ + \frac{\sqrt{3}\mu w}{4N^2} [\sin^2\theta_A \cos 2\varphi_A (3\cos^2\theta_B - 1) \\ + \sin^2\theta_B \cos 2\varphi_B (3\cos^2\theta_A - 1)] \\ + \frac{\mu^2}{4N^2} (3\cos^2\theta_A - 1)(3\cos^2\theta_B - 1) \end{pmatrix} \right\rangle$$

$$C_{-2} = (r^{\text{rigid}})^6 \left\langle \frac{1}{r_A^3 r_B^3} \left(\frac{3}{4} \sin^2\theta_A \sin^2\theta_B \sin 2\varphi_A \sin 2\varphi_B \right) \right\rangle$$

$$C_1 = (r^{\text{rigid}})^6 \left\langle \frac{1}{r_A^3 r_B^3} \left(\frac{3}{4} \sin 2\theta_A \sin 2\theta_B \sin \varphi_A \sin \varphi_B \right) \right\rangle$$

$$C_{-1} = (r^{\text{rigid}})^6 \left\langle \frac{1}{r_A^3 r_B^3} \left(\frac{3}{4} \sin 2\theta_A \sin 2\theta_B \cos \varphi_A \cos \varphi_B \right) \right\rangle$$

$$C_0 = (r^{\text{rigid}})^6 \left\langle \frac{1}{r_A^3 r_B^3} \begin{pmatrix} \frac{3\mu^2}{4N^2} \sin^2\theta_A \sin^2\theta_B \cos 2\varphi_A \cos 2\varphi_B \\ - \frac{\sqrt{3}\mu w}{4N^2} [\sin^2\theta_A \cos 2\varphi_A (3\cos^2\theta_B - 1) \\ + \sin^2\theta_B \cos 2\varphi_B (3\cos^2\theta_A - 1)] \\ + \frac{w^2}{4N^2} (3\cos^2\theta_A - 1)(3\cos^2\theta_B - 1) \end{pmatrix} \right\rangle \tag{15.1-5}$$

where the brackets indicate motional averaging. The indices A and B designate the K–L vector at time points 0 (A) and t (B). The following abbreviations are used:

$$D' = \sqrt{\frac{D_xD_y + D_xD_z + D_yD_z}{3}}; \quad D = \frac{D_x + D_y + D_z}{3}$$

$$\mu = \sqrt{3}(D_x - D_y); \quad w = 2D_z - D_x - D_y + 2\Delta$$

$$\Delta = 3\sqrt{D^2 - D'^2}; \quad N = 2\sqrt{\Delta w}$$

Specific effective correlation times and order parameters of fast motion are associated with every C_k coefficient:

$$\frac{1}{\tau_{\text{tot},j}} = \frac{1}{\tau_j} + \frac{1}{\tau_{\text{int}}} \tag{16}$$

$$S_{KL,j}^{\text{fast2}} \equiv \frac{C_j}{C_j^{\text{rigid}}} \tag{17}$$

C_k^{rigid} are the C_k coefficients under assumption of absence of internal motion and are considerably simpler:

$$\begin{aligned} C_2^{\text{rigid}} &= \frac{3w^2}{4N^2} \sin^4\theta \cos^2 2\varphi + \frac{\sqrt{3}\mu w}{2N^2} \sin^2\theta \cos 2\varphi (3\cos^2\theta - 1) \\ &\quad + \frac{\mu^2}{4N^2} (3\cos^2\theta - 1)^2 \\ C_{-2}^{\text{rigid}} &= \frac{3}{4} \sin^4\theta \sin^2 2\varphi \\ C_1^{\text{rigid}} &= \frac{3}{4} \sin^2 2\theta \sin^2\varphi \\ C_{-1}^{\text{rigid}} &= \frac{3}{4} \sin^2 2\theta \cos^2\varphi \\ C_0^{\text{rigid}} &= \frac{3\mu^2}{4N^2} \sin^4\theta \cos^2 2\varphi - \frac{\sqrt{3}\mu w}{2N^2} \sin^2\theta \cos 2\varphi (3\cos^2\theta - 1) \\ &\quad + \frac{w^2}{4N^2} (3\cos^2\theta - 1)^2 \end{aligned} \tag{18.1-5}$$

For practical purposes these expressions are highly complex and underdetermined in any kind of experimental approach. One problem arises from the correlation between the vector length and orientation. In models for motional description of covalent bonds (e.g. H^N–N) independence can be safely assumed and the distance dependence is separated from the C_k coefficients. It has been shown that this approximation is also valid for many cases of ^{1}H–^{1}H NOEs [10] but in general care has to be applied. In the following this assumption is made to obtain more convenient expressions:

$$C_k = \left(r_{KL}^{\text{rigid}}\right)^6 \left\langle \frac{1}{(r_{KL})^3} \right\rangle^2 C_k^{\text{Y}} \tag{19}$$

For the majority of macromolecules, the assumption of axially symmetric rather than fully anisotropic tumbling is valid. In this limit $\tau_{-j} = \tau_j$ and

$$\begin{aligned} C_2^{\text{Y}} + C_{-2}^{\text{Y}} &= \frac{3}{4} \sin^4\theta \\ C_1^{\text{Y}} + C_{-1}^{\text{Y}} &= 3\sin^2\theta\cos^2\theta \\ C_0^{\text{Y}} &= \left(\frac{3\cos^2\theta - 1}{2}\right)^2 \end{aligned} \tag{20.1-3}$$

and

$$\begin{aligned} 1/\tau_{\pm 2} &= 4D_{\text{II}} + 2D_{\perp} \\ 1/\tau_{\pm 1} &= D_{\text{II}} + 5D_{\perp} \\ 1/\tau_0 &= 6D_{\perp} \end{aligned} \tag{21.1-3}$$

Even under these simplifying conditions, fast motion of the vector samples orientations associated with varying impact of τ_k. In this study S_{KL}^2 is calculated using the exact solution for anisotropic tumbling of a rigid molecule (Eq. (9)). However, to implement a specific motional model, it is instructive to modify the predicted rigid cross-relaxation rate by a relative change calculated from a model assuming isotropic tumbling rather than Eq. (15.1-5). This approach has previously been applied to the prediction of cross-correlated relaxation rates in an anisotropically tumbling GB3 [14].

3. Experimental section

3.1. Sample expression and purification

GB3 was expressed and purified as described previously [15]. The ^{13}C,^{15}N-labeled and deuterated (non-perdeuterated) ^{2}H,^{13}C,^{15}N-labeled NMR samples contained 350 μl of 4 mM and 500 μl of 2 mM protein solution, respectively, in 95% H_2O, 5% D_2O, 50 mM potassium phosphate buffer, pH 6.5, and 0.5 mg/ml sodium azide.

^{13}C,^{15}N-labeled and perdeuterated ^{2}H,^{13}C,^{15}N-labeled ubiquitin was expressed and purified as described previously [3]. The NMR samples contained 400 μl of 4.3 mM protein solution in 97% H_2O, 3% D_2O, at pH 5.8.

3.2. NMR spectroscopy

All experiments were performed on Bruker 700 and 900 MHz spectrometers equipped with a triple resonance cryoprobe. Spectra were processed with the programs PROSA [16] or NMRPipe [17] and analyzed with the programs XEASY [18] and NMRDraw [17].

The following experiments were used to measure NOE buildup rates (see Table 1): a 3D ^{15}N-resolved HMQC–NOESY experiment [3] with a WATERGATE element for water suppression [4] for ^{2}H,^{13}C,^{15}N-labeled ubiquitin (mixing times t_{mix} = 30, 60, 90, and 200 ms at 700 MHz), ^{2}H,^{13}C,^{15}N-labeled GB3 (t_{mix} = 30, 40, 50, and 60 ms at 700 MHz) and ^{13}C,^{15}N-labeled GB3 (t_{mix} = 30, 40, 50, and 60 ms at 900 MHz); a 3D ^{15}N-resolved NOESY–HSQC experiment with STATES-TPPI acquisition mode in the ^{15}N dimension [19] and a trim pulse before acquisition [20] for ^{2}H,^{13}C,^{15}N-labeled GB3 (t_{mix} = 30, 40, 50, and 60 ms at 900 MHz); a 3D ^{15}N-resolved NOESY–HMQC experiment [19] with a WATERGATE element for water suppression [4] for ^{13}C,^{15}N-labeled ubiquitin (mixing times t_{mix} = 10, 15, 20, and 25 ms at 700 MHz).

3.3. Order of elements in the HMQC–[^{1}H,^{1}H]–NOESY and [^{1}H,^{1}H]–NOESY–HMQC/HSQC pulse sequences

The intensity of detected ^1H_j magnetization I_{ij}^{det} originating from the initial ^1H_i magnetization with intensity I_i^{init} can be expressed as follows for HXQC–NOESY [3]:

$$I_{ij}^{det}(t_{mix}) = \alpha_i^{rec} \cdot I_i^{init} \cdot T_{ii}^{HXQC} \cdot T_{ij}^{NOESY}(t_{mix}) \cdot T_{jj}^{WG}, \quad \alpha_i^{rec} \leqslant 1 \qquad (22.1)$$

and for NOESY–HXQC

$$I_{ij}^{det}(t_{mix}) = \alpha_i^{rec} \cdot I_i^{init} \cdot T_{ij}^{NOESY}(t_{mix}) \cdot T_{jj}^{HXQC}, \quad \alpha_i^{rec} \leqslant 1 \qquad (22.2)$$

α_i^{rec} denotes the part of the magnetization that has recovered during the interscan delay, T_{ii}^{HXQC} the loss of magnetization during the HXQC element, T_{jj}^{WG} the loss of magnetization during the WATERGATE element [4] before acquisition, and T_{ij}^{NOESY} is described by Eq. (3.1) for $i \neq j$ and by Eq. (3.2) for $i = j$, respectively.

If the NOESY is placed after the HXQC element relaxation during HXQC is identical for the diagonal and every of its NOESY cross peaks since they share the same magnetization pathway. Slight ^1H_j dependence during T_{jj}^{WG} can be neglected by the assumption that it is identical for all j during the short period. In case this assumption is invalid it would be reflected in the experimental error. T_{ij}^{NOESY} can now be extracted by normalization of the cross-peak intensities ($i \neq j$) by the diagonal peak intensity ($i = j$) at $t_{mix} = 0$:

$$T_{ij}^{NOESY}(t_{mix}) = \frac{I_{ij}^{det}(t_{mix})}{I_{ii}^{det}(0)} \qquad (23)$$

The advantage of this approach is that σ_{ij} and σ_{ji} are obtained independently and can be used for error estimation. In addition, if one of the pathways cannot be evaluated (e.g. due to peak overlap) the NOE can still be obtained. However, there is an error expected from the assumption of identical T_{jj}^{WG}. Furthermore, if the determination of quantitative NOEs is expanded to aliphatic protons, the WATERGATE sequence suppresses in part the $^1H^{\alpha}$ signals which would result in a frequency-dependent T_{jj}^{WG} value and hence the uniformity assumption is not valid anymore.

This problem can be largely bypassed by reversing the order of the elements. Having the HXQC element preceding acquisition water signals can be suppressed by gradient coherence selection or/and by the use of trim pulses [20] just before acquisition. $T_{ij}^{NOESY} = T_{ji}^{NOESY}$ can be extracted by the following normalization using both cross-peak intensities ($i \neq j$) and both diagonal peak intensities ($i = j$) at $t_{mix} = 0$:

$$\sqrt{\frac{I_{ij}^{det}(t_{mix}) I_{ji}^{det}(t_{mix})}{I_{ii}^{det}(0) I_{jj}^{det}(0)}} = T_{ij}^{NOESY}(t_{mix}) = T_{ji}^{NOESY}(t_{mix}) \qquad (24)$$

Note that this approach could also be used for the HXQC–NOESY if T_{jj}^{WG} is not sufficiently identical. This approach gives theoretically the exact solution but the random error cannot be estimated. If one of the cross peaks is missing no value can be obtained or a larger error has to be tolerated. Unfortunately, in practice this situation is met frequently.

3.4. Corrections for temperature differences

The data sets are recorded at different temperatures (Table 1). In order to compare cross-relaxation rates and distances obtained from the various experiments corrections must be applied [23]. In the following, all correlation times at experimental temperatures T_{exp} are estimated from those reported in the literature for temperature T_{lit} as

$$\tau_c(T_{exp}) = \frac{\eta(T_{exp}) T_{lit}}{\eta(T_{lit}) T_{exp}} \tau_c(T_{lit}) \qquad (25)$$

with $\eta(T)$ being the viscosity of water at temperature T. For GB3, the tensors from Ref. [22] are used and for ubiquitin from reference [21] and scaled to match those reported in reference [3] which was obtained from the program DASHA [24]. For comparison of cross-relaxation rates, the experimental values are scaled accordingly to the expected value at T = 297 K for GB3 and 300 K for ubiquitin.

Table 1
NOESY experiments conducted.

Code	Protein	Labeling	Pulse sequence	Field (MHz)	Temp. (K)	# Cross peaks	# Cross-relaxation rates[a]	rmsd (Hz)[b]
A	GB3	^{2}H,^{13}C,^{15}N	HMQC–NOESY (WG)[c]	700	291	116	77 (40)	0.035
B	GB3	^{2}H,^{13}C,^{15}N	NOESY–HSQC (TP)[d]	700	291	109	72 (38)	0.082
C	Ubiquitin	^{2}H,^{13}C,^{15}N	HMQC–NOESY (WG)[c]	700	284	215	138 (77)	0.061[e]
D	GB3	^{13}C,^{15}N	HMQC–NOESY (WG)[c]	900	293	122	74 (48)	0.063
E	Ubiquitin	^{13}C,^{15}N	HMQC–NOESY (WG)[c]	700	278	150	90 (60)	0.080

[a] Number of spin pairs for which at least one rate could be obtained; in parentheses number of spin pairs for which both rates could be obtained.
[b] Root-mean-square deviation over all spin pairs for which both cross peaks could be fitted.
[c] Water suppression is achieved with a WATERGATE sequence [4].
[d] Water suppression is achieved with a trim pulse preceding acquisition [20].
[e] Spin pair 35–36 omitted.

4. Results and discussion

It is the aim of the presented study to discuss various aspects important for the determination of quantitative NOEs and derived distances thereof. These include sample preparation aspects, spin diffusion, the pulse sequences, and the influence of anisotropic tumbling of the proteins. These criteria are discussed both from a theoretical and an experimental point of view using the two well-characterized model proteins GB3 and ubiquitin (Tables 2 and 3).

4.1. Cross-relaxation rate prediction with anisotropic tumbling

Anisotropic tumbling of the molecule can have a significant impact on the prediction of cross-relaxation rates based on a structure. Fig. 3 shows the variability (ratio between the maximal and minimal value) of the spectral density function and the effective distance for a rigid molecule in dependence on the anisotropy of tumbling. For simplicity axially symmetric tumbling is assumed where the anisotropy is expressed as $D_{\parallel}/D_{\perp}$. If the isotropic tumbling model is used the predicted value falls approximately between the two extremes and maximal errors can be estimated.

As pointed out previously for ubiquitin the error for the spectral density is smaller than 5% [3]. Nevertheless, in this study, a symmetric diffusion tensor is used with a ratio of the main axis to the averaged perpendicular axis $D_{\parallel}/D_{\perp}$ of ≈1.17 at T = 300 K [21]. Very accurate diffusion tensors for GB3 at T = 297 K are available from Ref. [22]. $D_{\parallel}/D_{\perp}$ is ≈1.4 and there is a small rhombic component. It has been demonstrated on the ^{15}N,^{13}C-labeled sample used here that this tensor predicts cross-correlated cross-relaxation rates very accurately and improves the agreement with experimental data when switching from the isotropic to the symmetric and finally the fully anisotropic model [14]. (Note: the temperatures during the measurements in this study deviate from those used for the diffusion tensor determination. The tensors were corrected for temperature effects by assuming that all components change uniformly.) Fig. 4 shows a correlation plot between cross-relaxation rates predicted with an isotropic and fully anisotropic tumbling for GB3. The error can become as large as 10% (Fig. 3A). If order parameters are calculated (Eq. (9)) the anisotropy has to be accounted for. If the effective distance is calculated from an experimental cross-relaxation rate the error is significantly smaller (Fig. 3B). For ubiquitin the error is less than 0.5% and for GB3 1.5%, respectively.

Table 2
Slopes s and Pearson's correlation coefficients r between apparent H^N–H^N cross-relaxation rates σ_{KL}^{app} of GB3 originating from different experiments.

Dataset x axis	Dataset y axis[b]	Spin diffusion correction	s	r
A	B	No	1.007 (1.014)[a]	0.992 (0.994)[a]
A	B	Yes	1.007 (1.013)[a]	0.993 (0.994)[a]
A	D	No	1.035	0.987
A	D	Yes	1.015	0.987
B	D	No	1.034 (1.034)[a]	0.980 (0.994)[a]
B	D	Yes	1.013 (1.017)[a]	0.981 (0.994)[a]

[a] Only for spin pairs for which both cross peaks could be evaluated in B.
[b] Rates obtained from D extrapolated to T = 293 K.

Table 3
Slopes s and Pearson's correlation coefficients r between apparent H^N–H^N cross-relaxation rates σ^{app} of ubiquitin originating from different experiments.

Dataset x axis	Dataset y axis	Spin diffusion correction	s	r
C	E [a]	No	0.972[a]	0.968
C	E [a]	Yes	0.970[a]	0.971

[a] Rates extrapolated to T = 284 K.

4.2. Validation of pulse sequences

The analysis procedures introduced in the experimental section enable accurate cross-relaxation rate determination with both experiments proposed (i.e. the HXQC–NOESY and the NOESY–HXQC). To assess experimentally the effects of swapping the HXQC and the NOESY elements both pulse sequences were run and analysed with the triple-labeled GB3 sample (Table 1, A and B). The slope in a correlation plot deviates by 1% from 1 and Pearson's correlation coefficient is 0.99 (Fig. 5, Table 2). This shows that virtually no systematic error is introduced by swapping. If the cross-relaxation rates in both transfer directions are determined individually without using Eq. (24) for the NOESY–HSQC experiment, the rmsd between the two symmetric rates of the latter experiment is 0.82 s^{-1} which is twice as large as 0.35 s^{-1} obtained for the HXQC–NOESY experiment. This is caused by the fact that in the HXQC–NOESY experiment only spectral noise and the different relaxation pathways during the WATERGATE element contribute to the rate difference whereas an additional difference in relaxation is introduced during the HXQC element in experiment B. If only one of the cross peaks can be used this error must be tolerated. However, if both cross peaks can be evaluated Eqs. (23) and (24) can be used and the obtained NOE rates are equally accurate as those from the HXQC–NOESY experiment.

4.3. Validation of cross-relaxation rates from differently labeled samples

It is highlighted in the theory section that the labeling pattern of the protein samples may affect strongly the accuracy and precision of the determined NOE rates. Deuteration reduces spin diffusion and therefore smaller structure-based correction factors must be considered. Furthermore, longer mixing times are possible resulting in a larger number of NOE rates. On the other hand, if the exact deuteration level and distribution is not known (for example in deuterated, but non-perdeuterated samples) spin-diffusion-related correction factors are not exact and NOE rates from double-labeled samples may be more accurate, in particular if very short mixing times are used. To validate experimentally these theoretical considerations cross-relaxation rates obtained from ^{13}C,^{15}N- and deuterated (non-perdeuterated) ^{13}C,^{15}N-labeled samples of GB3 and ^{13}C,^{15}N- and perdeuterated ^{13}C,^{15}N-labeled samples of ubiquitin are compared to each other, respectively (Figs. 6 and 7, Tables 2 and 3).

For GB3 equally long mixing times (maximally 60 ms) in all experiments for both samples were used. The effect of spin diffusion causes rates obtained from the protonated sample appear to be on average 3.5% larger than those from the deuterated sample after correction for the slightly different measurement temperatures. The corresponding correlation coefficients are high (≈0.980; Table 2). Upon taking into account spin diffusion the average difference reduces to 1.5% between rates from double and triple-labeled samples. The correlation only notably improves for corrections on small rates (>0.2 s^{-1}) as shown in Fig. 7 and therefore the correlation coefficients are very similar. The residual difference may be caused by individual rates. The three strongest outliers all involve the diagonal peak of residue 35 which strongly overlaps with the one of residue 15 in experiment D (spin pairing

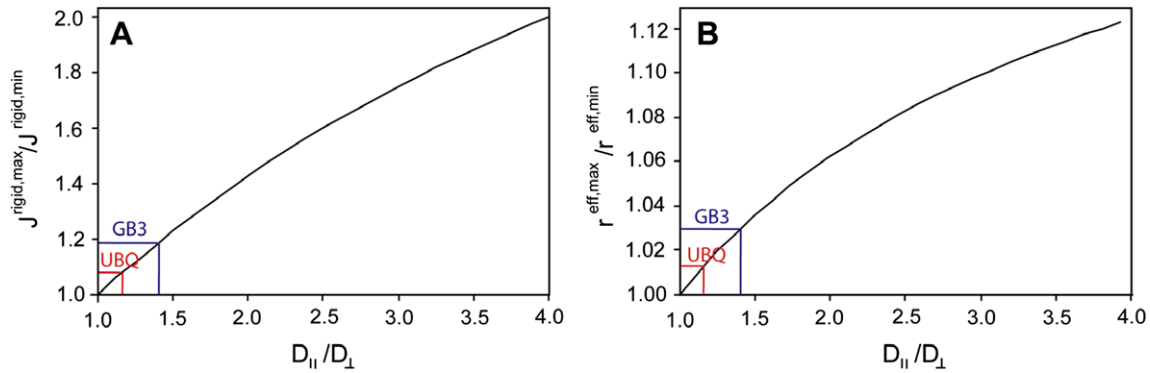

Fig. 3. Variability of the spectral density J^{rigid} (A) and effective distance r^{eff} (B) of a rigid molecule versus the diffusion anisotropy $D_{II}/D_{\perp}$. The variability is expressed as the maximal divided by the minimal value. The values for ubiquitin and GB3 are indicated in red and blue, respectively. (For interpretation of the references to color in this figure legend, the reader is referred to the web version of this article.)

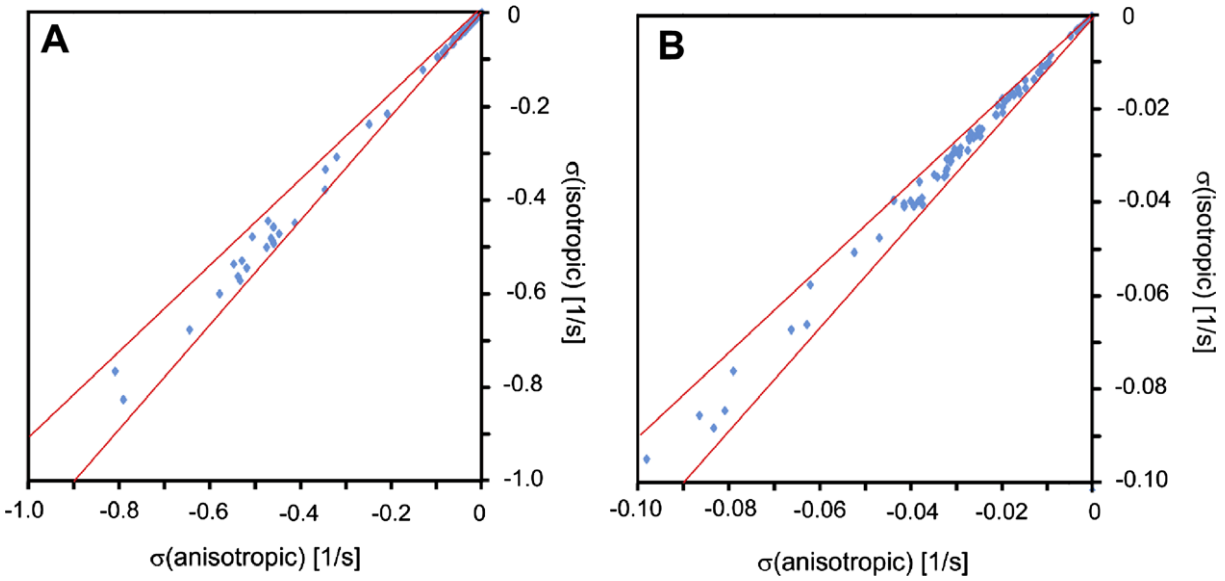

Fig. 4. Correlation plots of cross-relaxation rates σ_{KL} predicted for isotropic and fully anisotropic tumbling of GB3 at large scale (A) and small scale (B). The protein is assumed to be rigid. Diffusion tensors are taken from Ref. [22]. The red lines indicate slopes of 0.9 and 1.1 indicating the ±10% interval. (For interpretation of the references to color in this figure legend, the reader is referred to the web version of this article.)

with residues 33, 34, 36 and 39). These outliers are therefore to be categorized as artifacts. Why these build ups have not been identified and discarded during the initial analysis of the spectra is unclear, but may be attributed in part to the semi-automatic analysis process.

The situation is somewhat different in the case of ubiquitin (Table 3). The rates obtained from the protonated sample appear smaller than those from the perdeuterated sample. This is a trend opposite to the one expected from spin diffusion. It is likely that the much larger temperature correction deviates substantially from the true viscosity difference and correspondingly the rotational correlation time, which to first order proportionally influences the cross-relaxation rates (see also below for further discussions). Indeed, the correlation coefficient (which is not affected by the different temperatures used) is high (0.968). This data comparisons suggest that $^{1}H^{N}$–$1H^{N}$ NOE rates can be extracted with similar precision from both a ^{13}C,^{15}N- or a perdeuterated ^{13}C,^{15}N-labeled ubiquitin if for the double-labeled sample short NOE mixing times (in the case of ubiquitin up to 25 ms only) are used to reduce the unwanted spin diffusion (Fig. 2). Indeed, the slope and the correlation coefficient between the two data sets do not change significantly upon correction for spin diffusion with notable improvement for small rates (>0.2 s^{-1}) only (see Fig. 7). In turn, the short mixing times requested for double-labeled samples result in a reduced number of cross peaks, which in the case of ubiquitin drops by around 30% (Table 1).

4.4. Validation of distances

The cross-relaxation rates are converted into effective distances assuming an isotropically tumbling and rigid molecule following Eq. (12). The extremely good agreement between these distances obtained from different experiments and samples used is presented in Tables 4 and 5. For GB3 the slope between the data set A and B differs by 1% from 1 (Table 4). Apparent distances obtained from the double-labeled sample (experiment D) are 2% smaller than those from the triple-labeled samples (experiments A and B) because of stronger spin diffusion. Interestingly, all correlation coefficients are lower than those for the cross-relaxation rates. Apparently, taking the inverse sixth power causes a larger spread for small rates with relatively large uncertainties. When repeating the statistics for distances rather than cross-relaxation rates, cor-

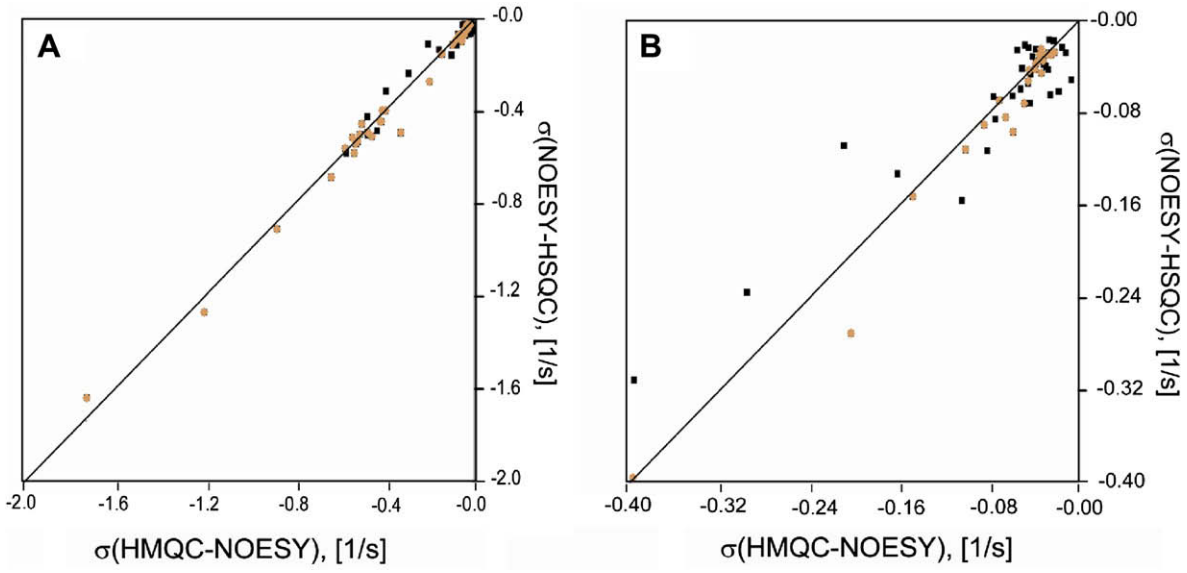

Fig. 5. Correlation plots of cross-relaxation rates σ_{KL} of triple-labeled GB3 obtained from HMQC–NOESY to NOESY–HSQC pulse sequences (extrapolated to $T = 295$ K). Corrections for spin diffusion have been applied as described in Ref. [3]. A shows the complete range and B a blow up of small rates. Rates are either obtained only if both cross peaks in NOESY–HSQC (orange diamonds) or if at least one cross peak could be fitted (black squares). The black line has a slope of 1. A linear regression deviates 1% from 1 and Pearson's correlation coefficient is 0.99. Note that the same statistics hold for uncorrected rates since the same sample and mixing times were used. (For interpretation of the references to color in this figure legend, the reader is referred to the web version of this article.)

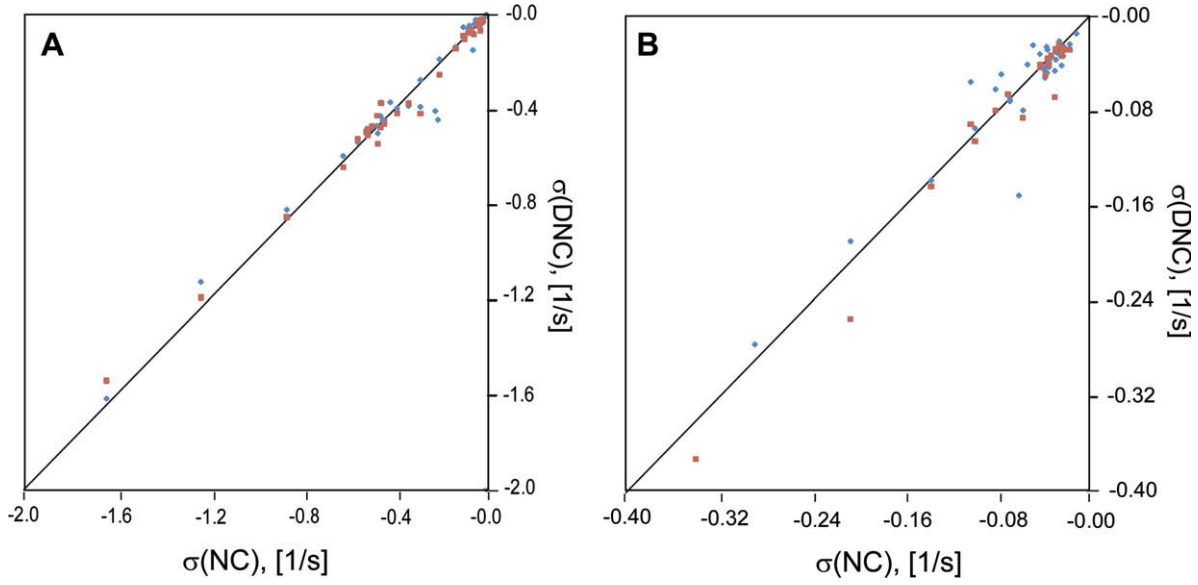

Fig. 6. Correlation plots of cross-relaxation rates σ_{KL} of GB3 obtained from double and triple-labeled samples. Corrections for spin diffusion have been applied as described in Ref. [3]. The rates of the triple-labeled sample are extrapolated to $T = 293$ K. A shows the complete range and B a blow up of small rates. Rates are obtained from experiment D and either A (HMQC–NOESY, blue diamonds) or B (NOESY–HSQC, only if both cross peaks could be fitted, purple squares). The black line has a slope of 1. (For interpretation of the references to color in this figure legend, the reader is referred to the web version of this article.)

rections for spin diffusion may play a more dominant role. Effective GB3 distances obtained from A and B are plotted versus those from D in Fig. 8. As for the cross-relaxation rates, in GB3, there is virtually no change in the correlations between A and B since all rates are affected similarly. Comparing double and triple-labeled samples shows that triple-labeled sample have smaller apparent distances than double-labeled samples whereas before the correction they were somewhat larger. This is caused by the larger rescaling of the rates from the double-labeled samples.

Similarly for ubiquitin, apparent distances obtained from the double-labeled sample (experiment E) are 5% smaller than those from the triple-labeled sample (experiment C) (see Table 5). Upon correction for spin diffusion, the underestimation of the distances from the double-labeled sample is reduced from 4.6% to 2.5%, whereas the correlation is slightly worse. Overall, because of the inverse sixth power relationship between the distance and the cross-relaxation rate (Eq. (5)) the extracted distances are not strongly dependent on the pulse sequences used or the samples

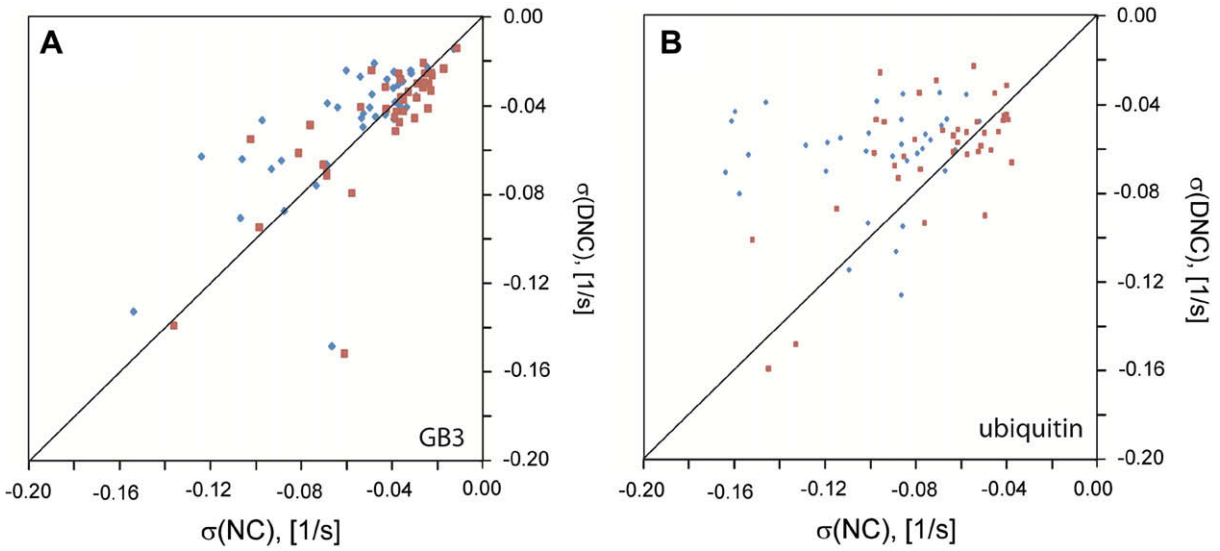

Fig. 7. Impact of correction for spin diffusion shown for the relevant rate range. Correlation plots of cross-relaxation rates σ_{KL} of GB3 (A) and ubiquitin (B) obtained from double (NC, experiments D and E) and triple-labeled samples (DNC, experiments A and C) after correcting for temperature differences. The rates are compared before (blue diamonds) and after applying corrections for spin diffusion (purple squares). The range is chosen such that rates for which the corrections have the largest impacts are on display. All rates are obtained from HMQC–NOESY with WATERGATE. The black line has a slope of 1. (For interpretation of the references to color in this figure legend, the reader is referred to the web version of this article.)

Table 4
Slopes s and Pearson's correlation coefficients r between apparent H^N–H^N distances r^{app}_{HN-HN} of GB3 originating from different experiments.

Dataset x axis	Dataset y axis	Spin diffusion correction	s	r
A	B	No	0.988 (0.993)[a]	0.990 (0.956)[a]
A	B	Yes	0.989 (0.993)[a]	0.991 (0.957)[a]
A	D	No	0.974	0.962
A	D	Yes	1.009	0.971
B	D	No	0.985 (0.980)[a]	0.980 (0.945)[a]
B	D	Yes	1.017 (1.015)[a]	0.986 (0.958)[a]

[a] Spin pairs for which one or both cross peaks could be evaluated for B and E.

Table 5
Slopes s and Pearson's correlation coefficients r between apparent H^N–H^N distances r^{app}_{HN-HN} of ubiquitin originating from different experiments.

Dataset x axis	Dataset y axis	Spin diffusion correction	s	r
C	E	No	0.954	0.950
C	E	Yes	0.982	0.955

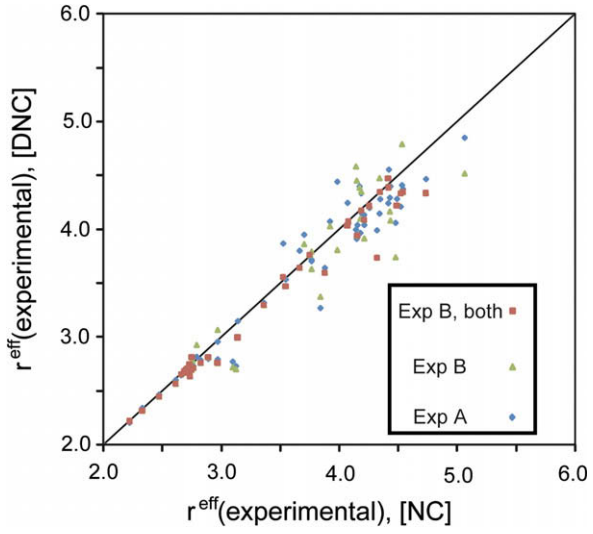

Fig. 8. Correlation plots of experimental effective distances r of GB3 obtained from the triple versus those from double-labeled sample. Corrections for spin diffusion have been applied as described in Ref. [3]. Distances are obtained from the triple-labeled sample using experiment A (HMQC–NOESY, blue diamonds) or B (NOESY–HSQC, only if both cross peaks could be fitted, purple squares, and also including single cross peaks, green triangles). Isotropic tumbling is assumed. The black line has a slope of 1.

used although they may have extensively different spin diffusion pathways.

4.5. Validation of the NOE-derived distances by atomic-resolution structures

It is the aim of this paragraph to validate the measured NOE relaxation rates by those extracted from available 3D atomic-resolution structures. For this purpose, the NOE-derived distances are compared to those extracted from the high-resolution X-ray/NMR structure 2OED [15] with RDC-refined backbone proton positions [25,26] of GB3 and the 1.8 Å resolution X-ray structure 1UBQ of ubiquitin [27]. The GB3 hybrid structure has been shown to cross-validate best with $^3J_{HNH\alpha}$ scalar couplings [26,28] and $D_{HNH\alpha}$ RDCs [29]. In the X-ray structure the amide protons were placed at ideal positions with 1.01 Å H–N bond length using the program MolMol [30]. The cross-relaxation rates are compared here with single structures rather than with ensemble representations [31–33] since in the case of ubiquitin the latter did not fit better the NOE data [3]. The NOE-derived distances are calculated under the assumption of an isotropically tumbling and rigid molecule following Eq. (12). The anisotropy of the molecule is neglected because it does hardly influence the distance determination due to the power of six dependence between the NOE and the distance

(see Fig. 3). Furthermore, in the course of an NMR structure determination distance extraction from NOEs cannot rely on the knowledge of anisotropy because of the lack of a structure available (note, this problem could be circumvented if necessary, since the anisotropy could be incorporated during the refinement of the structure determination).

Pearson's correlation coefficients and slopes obtained from comparison of experimental effective distances r^{eff} of GB3 with those calculated from the 3D structure are presented in Table 6 and plotted in Fig. 9. The slopes deviate less than 1% for all experiments. Generally, reliable NOEs can be obtained from experiments with the HXQC before acquisition and from experiments conducted at temperatures for which the correlation time is estimated using Eq. (25). Since the influence of spin diffusion on the distances is in average only 4%, the distances obtained from the double-labeled sample (experiment D) are as accurate as those obtained from the triple-labeled sample (experiments A and B). This finding opens the door to extraction of exact distances between any protons in a protein.

The same statistics for ubiquitin are shown in Table 7. Again, the slopes for the triple and double-labeled sample are remarkably close to 1. When no correction for spin diffusion is applied, the distances are underestimated on average by 0.4% and 4.2% for the triple and double-labeled sample, respectively. As shown in reference [3], for the triple-labeled sample this is mostly caused by distances between non-consecutive residues. Conclusively, for most cases exact distances can be extracted for both double and triple-labeled samples even without accounting for spin diffusion.

4.6. Extraction of dynamics from NOE rates

If a single 3D structure is a true average representation of the conformational ensemble, a comparison between cross-relaxation rates extracted from the NOE build ups and those calculated from the structure enables the determination of through space motional disorder described by the order parameter S^2_{KL} as defined by Eq. (9) [3]. However, the available structures may not be true average representations of the conformational ensemble and contain structural uncertainties and errors. Furthermore, weak NOE rates as well as the rotational correlation time of the protein may not be determined with high accuracy. Because the order parameter is proportional to both of them, it may also not be determined with high accuracy. Nevertheless, a motional network map may be established. Fig. 10 shows a correlation plot between experimental and predicted cross-relaxation rates of GB3 and Table 8 presents statistics characterizing the correlations. The analysis is carried out for all spin pairs, and several subgroups such as exclusively consecutive or non-consecutive residues and secondary structure elements. In all cases Pearson's correlation coefficient is larger for the anisotropic than for the isotropic tumbling model. The slopes

Table 6
Slopes s and Pearson's correlation coefficients r between experimental effective r^{eff}_{HN-HN} and theoretical r_{HN-HN} of GB3. Isotropic tumbling is assumed. Experimental distances are plotted on the x axis.

Experiment	Correction	r	s
A	Yes	0.922	1.000
A	No	0.933	1.004
B[a]	Yes	0.965	0.994
B[a]	No	0.973	0.998
B[b]	Yes	0.912	1.008
B[b]	No	0.890	1.013
D	Yes	0.947	0.992
D	No	0.933	1.039

[a] Only NOEs for which both cross peaks could be used.
[b] NOEs for which at least one cross peak could be used.

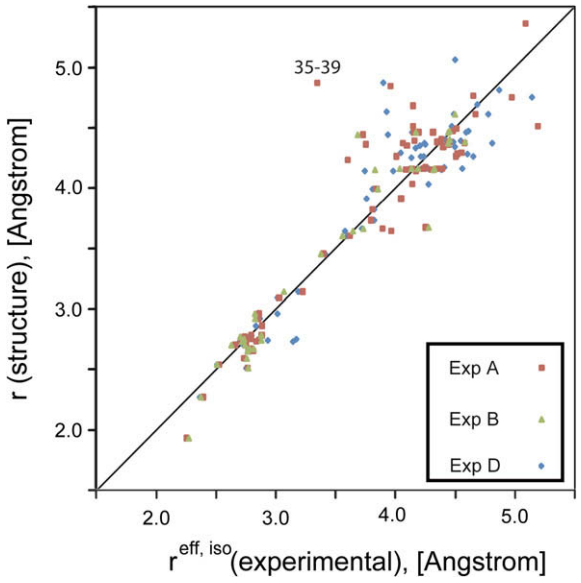

Fig. 9. Correlation plots of predicted and experimental distances r of GB3 obtained from double and triple-labeled samples. Corrections for spin diffusion have been applied as described in Ref. [3]. Distances are obtained from the triple-labeled sample using experiment A (HMQC–NOESY, purple squares) or B (NOESY–HSQC, only if both cross peaks could be fitted, green triangles) and the double-labeled sample (blue diamonds). Isotropic tumbling is assumed. Distance predictions are based on the structure with pdb code 2OED including improved protons positions. The black line has a slope of 1. τ_c is temperature corrected. (For interpretation of the references to colour in this figure legend, the reader is referred to the web version of this article.)

Table 7
Slopes s and Pearson's correlation coefficients r between experimental effective r^{eff}_{HN-HN} and theoretical r_{HN-HN} of ubiquitin. Isotropic tumbling is assumed. Experimental distances are plotted on the x axis.

Experiment	Correction	r	s
C	Yes	0.938	0.998
C	No	0.932	1.004
E	Yes	0.945	0.985
E	No	0.929	1.042

do not change significantly because either the proton–proton vectors are homogeneously distributed in angular space or they are not parallel to the largest or smallest main axis of the diffusion tensor. Of particular interest are the inverted slopes $1/s$, which are equivalent to averaged order parameters as defined in Eq. (9). For both triple-labeled and double-labeled GB3 samples, the averaged order parameter for all $^1H^N$–$1H^N$ NOEs is ≈0.85 and hence similar to order parameters from $^1H^N$–^{15}N vectors measured by conventional methods [13,19]. However, within the secondary-structural elements there is a 5–10% difference in the average order parameters between the two samples. This difference may be attributed in part to a non-accurate correction for spin diffusion in the double-labeled or triple-labeled samples. The values for consecutive residues in β strands and between β strands are larger than the others. The data on perdeuterated ubiquitin presented in Ref. [3] is reevaluated in Table 9. The overall average is ≈0.70. The statistics for the double labeled ubiquitin sample is in agreement with the results for the triple-labeled sample although an overall down-scaling of 5% is present. This may be attributed to not-accurate corrections for spin diffusion and correction for the temperature difference. The exceptions are the spin pairs between non-consecutive residues in the α helix. The values are ≈0.4 larger than those obtained from the triple-labeled sample. Within this set only four

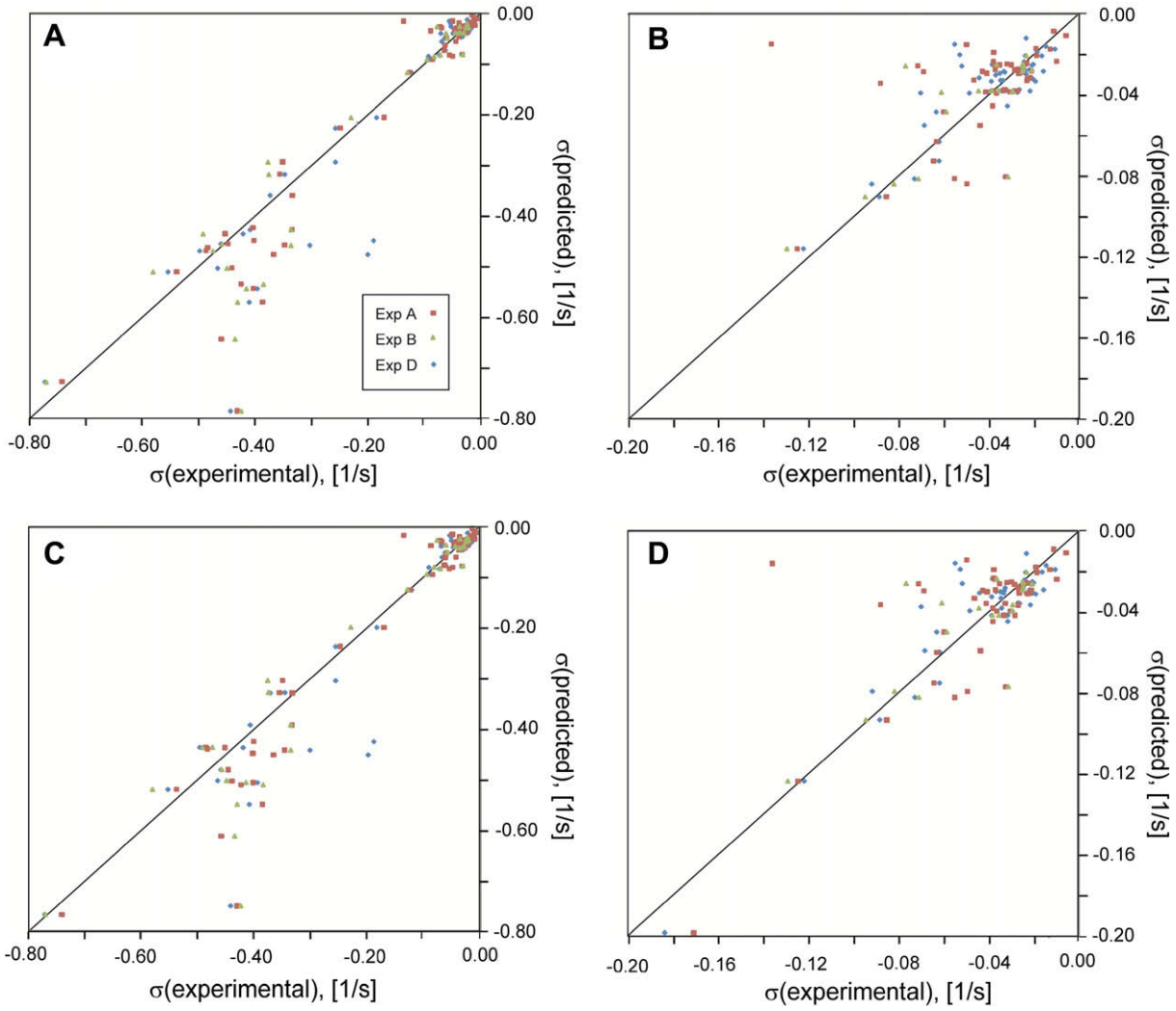

Fig. 10. Correlation plots of predicted and experimental cross-relaxation rates of GB3 obtained from double and triple-labeled samples. Corrections for spin diffusion have been applied as described in Ref. [3]. The rates are obtained from the triple-labeled sample using experiment A (HMQC–NOESY, purple squares) or B (NOESY–HSQC, only if both cross peaks could be fitted, green triangles) and the double-labeled sample (blue diamonds). Predictions are based on the structure 2OED with improved protons positions assuming isotropic tumbling (A and B) and anisotropic tumbling (C and D). The black line has a slope of 1. The effective τ_c is temperature corrected. (For interpretation of the references to color in this figure legend, the reader is referred to the web version of this article.)

cross-relaxation rates are obtained and they have a larger than usual spread and may not yield a reliable average. In detail, values much larger than those obtained from the triple-labeled sample are observed for the spin pairs 29/31 and 30/33. Corrections for spin diffusion are 25% and 17%, respectively, and possible errors of these cannot account for the effect. Interestingly, large cross-correlated chemical shift modulations between C^{α} and C^{β} have been observed for residues 31, 33 and 34 [34]. Such modulations are indicative of slow internal motion which may be insufficiently represented by a single conformer as used here. As observed for GB3, the values for consecutive residues in β strands are larger than the others. In contrast to GB3, however, this trend is not seen for pairs between β strands. The use of the anisotropic tumbling model does not improve Pearson's correlation coefficient. This is not surprising since ubiquitin has a significantly more isotropic diffusion tensor than GB3.

The overall difference between GB3 and ubiquitin may be attributed in part to an inaccurate determination of the rotational correlation time of the proteins, to protein-specific variations in dynamics, to the accuracy of the 3D structures used, and/or the accuracy of the deuteration levels assumed. In particular, the determination of the rotational correlation time may be questionable, since all cross-relaxation rates were scaled to those expected for the temperature at which the diffusion tensor and/or the effective tumbling time were determined (297 K for GB3 and 300 K/284 K for ubiquitin). It is possible that the simple relationship expressed in Eq. (25) is not sufficient for an exact adjustment. Furthermore, the error of ~10% of the effective tumbling time of ubiquitin at 284 K obtained from the simple relationship of the relaxation times T_1 and T_2 measured in [3] may influence the extraction of dynamics from NOEs accordingly by scaling the entire order parameters proportionally. The other source of error mentioned is the accuracy of the deuteration level, which is difficult to know in the absence of perdeuteration as in the case of the triple-labeled GB3. This lack of knowledge may result in errors in the order of up to 10% as well. Furthermore, such errors are distributed unevenly within the protein structure (Fig. 2). Finally, the accuracy of the 3D structure used may also influence the order parameters unevenly within the protein structure. In summary, although many parameters may result in errors that mask detailed motional insight, an overall qualitative similar behavior is observed for the secondary-structural elements of both GB3 and ubiquitin.

Table 8
Inverted slopes $1/s$ and Pearson's correlation coefficients r between spin diffusion and H/D equilibrium-corrected experimental and calculated H^N–H^N cross-relaxation rates σ of GB3 assuming isotropic and fully anisotropic tumbling. The inverted slope $1/s$ is also the averaged order parameter S^2_{KL}.

Experiment, model		All[a]	All consec.[a]	All non-consec.	Consec. β strand	Between β strands	Consec. α helix	Non-consec. α helix	Loops[a]
A, iso	*1/s*	0.852	0.831	0.913	1.129 [c]	0.968	0.883	0.927[e]	0.808
	r	0.967	0.971	0.940		0.937	0.407		0.969
A, aniso	*1/s*	0.870	0.849	1.001	1.103 [c]	0.978	0.906	0.918[e]	0.826
	r	0.973	0.977	0.946		0.945	0.639		0.975
B, iso	*1/s*	0.863	0.846	0.998	0.934 [d]	1.004	0.928	0.868	0.822
	r	0.957	0.956	0.944	0.382 [d]	0.905			0.967
B, aniso	*1/s*	0.872	0.864	1.000	0.904 [d]	1.006	0.948	0.836	0.839
	r	0.972	0.966	0.956	0.400 [d]	0.925			0.975
B[b], iso	*1/s*	0.877	0.851	1.042	1.008 [c]	1.013	0.904	0.823[e]	0.827
	r	0.962	0.966	0.948		0.949		0.699[e]	0.966
B[b], aniso	*1/s*	0.896	0.870	1.054	0.981 [c]	1.026	0.928	0.807[e]	0.845
	r	0.969	0.973	0.952		0.954		0.826[e]	0.975
D, iso	*1/s*	0.852	0.846	0.933	1.015[d]	0.893	0.842	0.880	0.847
	r	0.962	0.956	0.941		0.956		0.468	0.973
D, aniso	*1/s*	0.869	0.865	0.932	0.996[d]	0.891	0.861	0.873	0.866
	r	0.968	0.963	0.948		0.967		0.476	0.978

[a] Spin pair 11–12 omitted.
[b] All pairs of which at least one spin pair could be evaluated.
[c] Spin pairs 13–14 and 14–15 omitted.
[d] Spin pair 13–14 omitted.
[e] Spin pair 33–35 omitted.

Table 9
Inverted slopes $1/s$ and Pearson's correlation coefficients r between spin diffusion and H/D equilibrium-corrected experimental and calculated H^N–H^N cross-relaxation rates σ of ubiquitin assuming isotropic and fully anisotropic tumbling. The inverted slope $1/s$ is also the averaged order parameter S^2_{KL}.

Experiment, model		All[a]	All consec.[a]	All non-consec.	Consec. β strand	Between β strands	Consec. α helix	Non-consec. α helix	Loops[a]
C, iso	*1/s*	0.705	0.705	0.690	0.948	0.669	0.716	0.774	0.755
	r	0.969	0.961	0.969		0.981	0.275	0.601	0.950
C, aniso	*1/s*	0.701	0.700	0.688	0.942	0.667	0.710	0.775	0.749
	r	0.969	0.961	0.970		0.982	0.457	0.642	0.947
F, iso	*1/s*	0.672 [b]	0.671 [b]	0.700	1.053	0.653	0.777	*1.161* [c]	0.619 [b]
	r	0.970 [b]	0.965 [b]	0.956		0.970	0.768	*0.633* [c]	0.966 [b]
F, aniso	*1/s*	0.668 [b]	0.667 [b]	0.682	1.041	0.646	0.770	*1.148* [c]	0.616 [b]
	r	0.970 [b]	0.965 [b]	0.957		0.974	0.835	*0.871* [c]	0.963 [b]

[a] Spin pair 34–35 omitted.
[b] Spin pair 59–60 omitted.
[c] Poor statistics.

5. Conclusion

In this study errors and error sources for the extraction of $^1H^N$–$^1H^N$ NOE rates, average distances thereof and order parameters have been estimated at all stages from sample preparation to analysis. It is shown that distances can be determined accurately from both double and triple-labeled samples if for the double-labeled sample short mixing times are used. If it is the goal to extract also dynamics from NOE cross-relaxation rates either perdeuteration of the triple-labeled sample or double-labeling is advantageous. On the level of pulse sequences, NOESY–HXQC experiments provide rates of the same quality as HXQC–NOESY if both diagonal and cross peaks for a spin pair can be resolved. Expressions for cross-relaxation rates for anisotropically tumbling molecules exhibiting fast and slow motion have been derived. The impact of anisotropy on the prediction of cross-relaxation rates and on the conversion of experimental rates into effective distances can be neglected for exact distance measurements, whereas for dynamics analysis the effect of anisotropy should be included for a highly anisotropic molecule. Hence, the determination of accurate distances by NOE build up rates appears to be surprisingly robust. More delicate appears to be the determination of local dynamics *via* the order parameter S^2. Since the order parameter is also proportional to the rotational correlation time τ_c of the protein, τ_c must also be determined accurately. An error in τ_c will result thereby in an overall offset of the order parameters as demonstrated here for ubiquitin for which the extrapolation of τ_c seems to agree only within an error of 10%. Finally, "averaged order parameters" are calculated for specific secondary-structural elements and shown to have similar trends for ubiquitin and GB3. In summary, the quantitative determination of $^1H^N$–$^1H^N$ NOEs in both perdeuterated and double-labeled proteins is straightforward and enables the characterization of both the structure and the motion of a protein on a through-space level.

Acknowledgment

We thank Dr. Jason Greenwald for the preparation of the ubiquitin samples. This work was supported by the SNF.

Appendix A. Supplementary material

Table presenting corrections, cross-relaxation rates and effective distances obtained from experiments A and B for GB3; table presenting corrections, cross-relaxation rates and effective distances obtained from experiment D and theoretical distances and predicted cross-relaxation rates for GB3; table presenting corrections, cross-relaxation rates and effective distances obtained from

experiments C and E for ubiquitin; table presenting theoretical distances and predicted cross-relaxation rates for ubiquitin. Furthermore, a MATLAB code for calculation of spin diffusion can be downloaded from our webpage www.bionmr.ethz.ch. Supplementary data associated with this article can be found, in the online version, at doi:10.1016/j.jmr.2010.03.009.

References

[1] A. Kumar, G. Wagner, R.R. Ernst, K. Wüthrich, J. Am. Chem. Soc. 103 (1981) 3654–3658.
[2] S.W. Fesik, E.R.P. Zuiderweg, J. Magn. Reson. 78 (1998) 588–593.
[3] B. Vögeli, T.F. Segawa, D. Leitz, A. Sobol, A. Choutko, D. Trzesniak, W. van Gunsteren, R. Riek, J. Am. Chem. Soc. 131 (2009) 17215–17225.
[4] M. Piotto, V. Saudek, V. Sklenar, J. Magn. Reson. 2 (1992) 661–665.
[5] I. Solomon, Phys. Rev. 2 (1955) 559–565.
[6] D.M. LeMaster, Annu. Rev. Biophys. Biophys. Chem. 19 (1990) 243–266.
[7] D.M. LeMaster, Q. Rev. Biophys. 23 (1990) 133–174.
[8] K. Wüthrich, NMR of Proteins and Nucleic Acid, Wiley, New York, 1986.
[9] D. Neuhaus, M.P. Williamson, The Nuclear Overhauser Effect in Structural and Conformational Analysis, Wiley, New York, 2000.
[10] R. Brüschweiler, B. Roux, M. Blackledge, C. Griesinger, M. Karplus, R.R. Ernst, J. Am. Chem. Soc. 114 (1992) 2289–2302.
[11] G. Lipari, A. Szabo, J. Am. Chem. Soc. 104 (1982) 4546–4559.
[12] L.D. Favro, Phys. Rev. 119 (1960) 53–62.
[13] D.M. Korzhnev, M. Billeter, A.S. Arseniev, V.Y. Orekhov, Prog. Nucl. Magn. Reson. Spectrosc. 38 (2001) 197–266.
[14] B. Vögeli, L. Yao, J. Am. Chem. Soc. 131 (2009) 3668–3678.
[15] T.S. Ulmer, B.E. Ramirez, F. Delaglio, A. Bax, J. Am. Chem. Soc. 125 (2003) 9179–9191.
[16] P. Güntert, V. Dötsch, G. Wider, K. Wüthrich, J. Biomol. NMR 2 (1992) 619–629.
[17] F. Delaglio, S. Grzesiek, G.W. Vuister, G. Zhu, J. Pfeifer, A. Bax, J. Biomol. NMR 6 (1995) 277–293.
[18] C. Bartels, T.H. Xia, M. Billeter, P. Güntert, K. Wüthrich, J. Biomol. NMR 6 (1995) 1–10.
[19] J. Cavanagh, W.J. Fairbrother, A.G. Palmer, M. Rance, N.J. Skleton, Protein NMR Spectroscopy, Principles and Practice, Academic Press, San Diego, 2007.
[20] A. Bax, D.G. Davies, J. Magn. Reson. 5 (1985) 355–360.
[21] N. Tjandra, S.E. Feller, R.W. Pastor, A. Bax, J. Am. Chem. Soc. 117 (1995) 12562–12566.
[22] J.B. Hall, D. Fushman, J. Biomol. NMR 27 (2003) 261–275.
[23] S.L. Chang, N. Tjandra, J. Magn. Reson. 174 (2005) 43–53.
[24] V.Y. Orekhov, D.E. Nolde, A.P. Golovanov, D.M. Korzhnev, A.S. Arseniev, Appl. Magn. Reson. 9 (1995) 581–588.
[25] L. Yao, B. Vögeli, D.A. Torchia, A. Bax, J. Phys. Chem. B 112 (2008) 6045–6056.
[26] L.S. Yao, B. Vögeli, J.F. Ying, A. Bax, J. Am. Chem. Soc. 130 (2008) 16518–16520.
[27] S. Vijay-Kumar, C.E. Bugg, W.J. Cook, J. Mol. Biol. 194 (1987) 531–544.
[28] B. Vögeli, J.F. Ying, A. Grishaev, A. Bax, J. Am. Chem. Soc. 129 (2007) 9377–9385.
[29] B. Vögeli, L. Yao, A. Bax, J. Biomol. NMR 41 (2008) 17–28.
[30] R. Koradi, M. Billeter, K. Wüthrich, J. Mol. Graphics 14 (1996) 51–55.
[31] G.M. Clore, C.D. Schwieters, J. Mol. Biol. 355 (2006) 879–886.
[32] K. Lindorff-Larsen, R.B. Best, M.A. DePristo, C.M. Dobson, M. Vendruscolo, Nature 433 (2005) 128–132.
[33] O.F. Lange, N.A. Lakomek, C. Fares, G.F. Schröder, K.F.A. Walter, S. Becker, J. Meiler, H. Grubmüller, C. Griesinger, B.L. De Groot, Science 320 (2008) 1471–1475.
[34] D. Früh, J.R. Tolman, G. Bodenhausen, C. Zwahlen, J. Am. Chem. Soc. 123 (2001) 4810–4816.
[35] A. Kumar, R.C.R. Grace, P.K. Madhu, Prog. Nucl. Magn. Reson. Spectrosc. 37 (2000) 191–319.